Crystallization and Premelting in Thin Films of Weakly Interacting Molecules: A Study of Pyridine Films on Ag by Optical Second Harmonic Generation

Minchul Yang[†] and Hai-Lung Dai*

Department of Chemistry, University of Pennsylvania, Philadelphia, Pennsylvania 19104-6323

Received: May 7, 2003; In Final Form: September 3, 2003

It is shown that second harmonic generation from a thin molecular film can be used for characterizing the crystallization and premelting kinetics of the crystallites in the film. The new observations provide a model understanding of the growth and crystallization mechanism in thin films made of molecules, such as pyridine, with very weak intermolecular interactions. The amorphous pyridine films, with thickness less than 100 nm, deposited at 82 K under UHV conditions on Ag(111) are found to crystallize via a diffusion-limited process at temperatures above 120 K, forming polycrystallites through a cylindrical-plate shape. This shape suggests that film thickness is an important factor in determining the crystallization mechanism. The boundary of the polycrystallites in the annealed pyridine film is found to crystallize or melt reversibly with decreasing/increasing temperature in a temperature range (80−135 K) much lower than the bulk melting temperature and the film desorption temperature.

I. Introduction

Ultrathin molecular films with submicron thickness are currently of interest as a special class of materials with new technology applications. The recently developed organic semiconductors, which exist in the form of molecular thin films, promise a wide range of novel applications such as field effect transistors (FETs),[1,2] photodetectors,[3] photovoltaic devices,[4] and light-emitting diodes.[5] The molecular film materials have the advantages of being inexpensive and mechanically flexible. Furthermore, diversity of the molecular functional groups that can be built into the molecular thin films allows one to design new nonlinear optical materials.[6,7]

The utilization of the ultrathin molecular films in new electronic and optical devices has inspired the need for a fundamental understanding of their growth mechanisms, structures, and structural changes such as crystallization and premelting. For example, it has been recently suggested that performance in organic semiconductors is affected by grain boundaries which may limit the mobility of charge carriers inside the film.[8,9] A fundamental understanding of the film structure and structural dynamics is also important to the understanding of such phenomena as wetting, adhesion, friction, and lubrication, all long-standing issues in surface and interface science that are important to the mechanical properties of the film.[10] There has been great interest in this respect as enormous progress in micromechanical systems has been made in the study of nanotribology.[11,12]

As demonstrated in model systems of adsorption of rare gas atoms or diatomic molecules such as CO and N_2 on surfaces under ultrahigh vacuum (UHV) conditions,[13] the structure and growth of the submonolayer are determined by the properties of the constituent atoms/molecules, their intermolecular (atomic) interactions, the substrate structure, and the substrate−adsorbate interactions. The simple systems have made it possible to test theoretical models with an abundance of experimental data. In considering films made of molecules with the diversity of structures and intermolecular interactions, it is easy to imagine the complexity brought about by the nonisotropic molecular structures (orientation dependence) and intermolecular interactions with varying degrees of strength in determining the macroscopic properties of the film. Such characteristics highlight the importance of understanding the structure and structural changes in model systems.

We have chosen pyridine (C_5H_5N) films grown with submicron thickness on a flat Ag(111) surface under UHV conditions as a model system for studying structural transitions within thin molecular films. Pyridine is a simple, anisotropic, planar, aromatic molecule. Thin films of planar aromatic molecules such as (oligo)thiophene,[1,14] pentacene,[1,8,15] and perylene[7] are among the most promising materials for applications in photonics and organic semiconducting devices. The lack of inversion symmetry of the molecule also ensures a vector-like hyperpolarizability in the molecular frame and allows the use of optical second harmonic generation (SHG), a nonlinear optical technique, for characterizing the structure of the ensemble of the pyridine molecules in the film. As intermolecular interaction between pyridine molecules is particularly weak, 3.2 kcal/mol as measured as the strongest interaction between a pair of pyridine molecules,[16] the pyridine thin film also serves as a model system at the weak interaction end.

Characterizing the structure of thin molecular films under UHV conditions has been an experimentally challenging task. Temperature-programmed desorption (TPD) may reveal the desorption energy of the film, which is related to intermolecular interactions and orientational packing within the film. Surface analytical techniques including particle scattering and microscopic techniques, which are successful for surface or monolayer structure determination, on the other hand, do not have the probe depth for more than a few layers. Second harmonic generation (SHG), as a nonlinear optical technique, has a probe depth on the order of optical wavelength and is suitable for probing films

* To whom all correspondence should be addressed at the University of Pennsylvania. E-mail: dai@sas.upenn.edu.

[†] Present address: Department of Chemistry, University of California, Berkeley, CA 94720.

10.1021/jp0352478 CCC: $25.00
Published on Web 10/11/2003

with submicron thickness. In probing thin films composed of molecules with vector-like hyperpolarizability, SHG can reveal if the film structure is amorphous (or centrosymmetric), which yields no second harmonic signal, or if it has a crystalline structure but with no inversion symmetry, which generates a second harmonic (SH) signal. For the latter case, the light incident angle and polarization dependence of SHG can be used to reveal the alignment of the molecules in the film in the laboratory frame.

Previously it has been shown that SHG can be used to monitor the film growth rate[17] and that the pyridine film grown at liquid nitrogen cooled temperature (82 K) is amorphous but undergoes crystallization at 123 K in an annealing like process.[18] The ~100 nm thick pyridine film deposited on the surface, after annealing, shows that it consists of polycrystallites with the average diameter of the crystallite domains ≥600 nm and that the crystalline axis of the polycrystallites are isotropically and randomly oriented on the surface. In this report, we further demonstrate that SHG can be used to probe the crystallization kinetics within the thin film during the annealing process and detect the melting of the boundary of the polycrystallites as the temperature further increases. The new observations on the crystallization and premelting kinetics are consistent with the previous conclusions on the structure of the annealed pyridine films. Our results demonstrate the capability of the SHG technique for characterizing crystalline domains and grain-boundaries in ultrathin molecular films. The overall observations on this model pyridine film system illustrate how the structure changes within a film made of molecules with very weak intermolecular interactions.

II. Experimental Section

All experiments were performed in an ultrahigh vacuum (UHV) chamber with a base pressure of 2×10^{-10} Torr. The Ag(111) surface was cleaned routinely by several cycles of sputtering and annealing before experiment. Pyridine (>99.5%, Aldrich) was purified by several freeze−pump−thaw cycles before use. Pyridine molecules were deposited on the clean Ag(111) surface with use of a leak valve. The sample temperature was maintained within ±0.1 K during the deposition and optical measurement.

The 532-nm output from a Nd:YAG laser (Continuum 580A, 8 ns pulse length, 15 mJ/pulse in 4.5 mm diameter, linearly polarized with 60° incident angle) was used as the fundamental light in SHG. The SH light generated at the silver surface, propagating along with the fundamental light and exiting the pyridine film, was passed through a filter/monochromator assembly and detected by a photomultiplier. Detailed arrangement of the nonlinear optical experimental setup can be found elsewhere.[18]

III. Results and Analysis

A. Monitoring the Pyridine Film Growth Rate during Deposition. Optical interference in SHG in the system of a film on a surface can be used to measure the growth rate of the thin film. In the limit that SHG from the film is negligible in comparison with that from the surface, which is the case for an amorphous film, the film can be treated simply as an optically linear medium. The metal surface, such as Ag(111), due to reduced symmetry, is an intrinsic source for SHG in this system. The intensity of the second harmonic (SH) light generated at the surface and propagating through and exiting the pyridine film is detected at the specula angle. Both the SH and fundamental lights experience multiple reflections inside the film, resulting in the interference of these light fields. Consequently, the SH intensity as a function of film thickness exhibits oscillatory patterns as the film grows thicker.

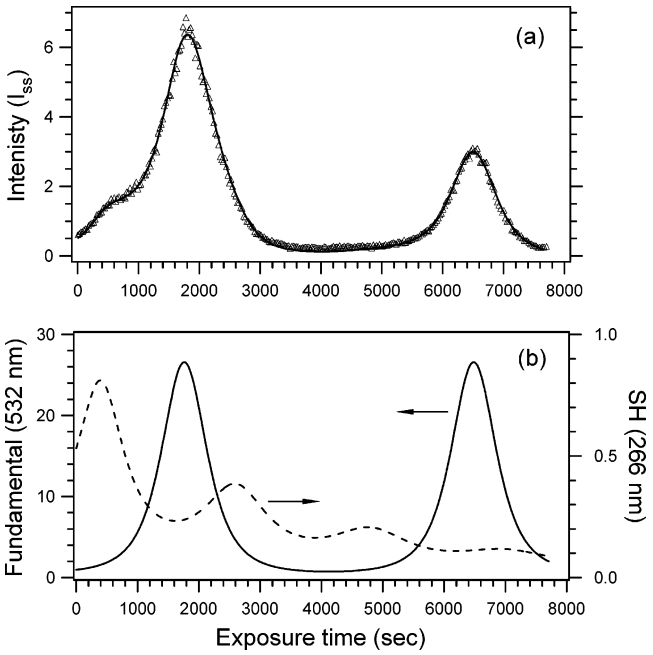

Figure 1. The SH intensity detected during deposition of pyridine thin film on Ag(111) at 82 K. The pressure of the pyridine vapor was fixed during the deposition at 5 (± 0.05) × 10^{-7} Torr, corresponding to 1.15 × 10^{14} molecules/(cm^2·s) in flux. In part a, open triangles are experimental results and the solid line is the fitting result using eqs 1 and 2. In part b, solid and dashed lines are respectively the contributions of the fundamental and SH lights to the overall SH intensity. I_{ss} denotes s-polarized SH light generated with s-polarized fundamental.

Variation of the SH intensity (open triangles) during pyridine deposition on the Ag(111) at 82 K is shown in Figure 1a as a function of exposure time. During the deposition, the pressure of the pyridine molecules was fixed at 5(±0.05) × 10^{-7} Torr, corresponding to 1.15 × 10^{14} molecules/(cm^2·s) in flux. The oscillatory pattern in the SH intensity with respect to exposure time is due to optical interference of both fundamental and SH lights within the pyridine film. One interesting feature in Figure 1a is that the second peak height is smaller than the first one. This is because overall the SH intensity decreases exponentially with increasing film thickness due to absorption of the 266-nm SH light by pyridine molecules through the n−π^* electronic transition at 4.5 eV.[19]

The detected SH intensity, $I^{2\omega}$, can be related to the SH intensity generated from the clean Ag(111) surface, $I_{Ag}^{2\omega}$, as

$$I^{2\omega} = \text{constant} \cdot |T_{02}^{\omega}|^4 |T_{20}^{2\omega}|^2 I_{Ag}^{2\omega} \quad (1)$$

Here T_{02}^{ω} is the transmission factor that describes the transmission of the fundamental light at frequency ω from the vacuum (medium 0), through the film (medium 1), onto silver (medium 2) and $T_{20}^{2\omega}$ is for the SH light at the frequency 2ω transmitting from silver to the vacuum. The transmission factors can be expressed as $[(t_{01}t_{12}e^{-i\delta})/(1 + r_{01}r_{12}e^{-2i\delta})]$, where t and r are transmission and reflection coefficients, respectively, relevant to the interfaces between media defined by the indices. The phase difference δ is defined as $(2\pi/\lambda)(n - ik)d$, where λ is the wavelength, d the thickness of the film, and n and k respectively the real and imaginary parts of the refractive index of the film. The imaginary part is introduced here to describe loss of light by scattering and absorption within the film.

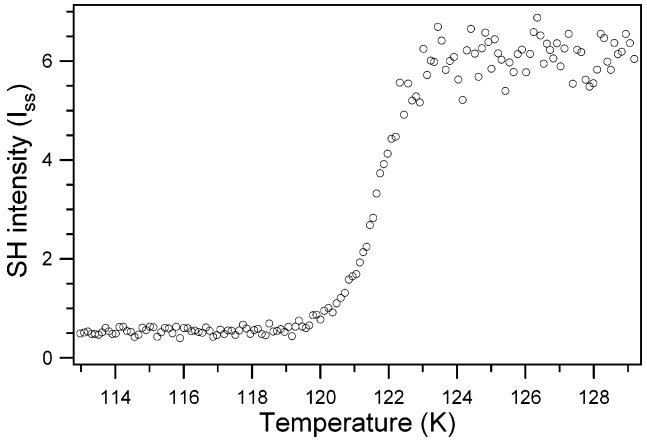

Figure 2. The SH intensity during annealing of a 140 nm thick amorphous pyridine film at a heating rate of 5 deg/min. The film was made at 82 K on Ag(111) by dosing for 1900 s at 5×10^{-7} Torr of pyridine pressure.

Assuming a film growth rate linearly proportional to exposure time during film deposition so that the growth rate G is related to the film thickness as $d = Gt$, we have

$$|T_{02}| = \left| \frac{t_{01}t_{12}e^{-(k+in)(2\pi/\lambda)Gt}}{1 + r_{01}r_{12}e^{-2(k+in)(2\pi/\lambda)Gt}} \right| \quad (2)$$

(Note that this equation is identical with eq 3 of ref 18 but the latter had a misprint in the sign in the denominator.) Equation 2 shows that $|T_{02}|$ displays periodicity of $[\lambda/(2Gn)]$ with exposure time. This oscillation in transmission factors for both the fundamental and SH lights results in the observed oscillatory pattern of SH intensity that can be used to deduce the growth rate—the film thickness as a function of exposure. In the case of loss of light by scattering or absorption within the film, $|T_{02}|$ would show an exponential decrease with a decay constant of $k(2\pi/\lambda)G$.

The solid line in Figure 1a is a nonlinear least-squares fit to eqs 1 and 2. The film growth rate obtained from the fitting is 0.77 Å/s at the prescribed pressure at 82 K. Figure 1b shows the individual interference oscillatory pattern of the fundamental and SH intensity separately, using the fitting results. It is important to note that the fitting patterns in Figure 1 are consistent with the assumption that the pyridine film grows on Ag(111) at 82 K as an amorphous solid that produces no SHG.

B. SH Intensity as a Function of Time and Temperature: Crystallization Kinetics. Figure 2 shows the change in the SH intensity as a function of temperature as a 140 nm thick amorphous pyridine film was annealed at a heating rate of 5 deg/min. The amorphous film was originally deposited on Ag(111) at 82 K after dosing for 1900 s at 5×10^{-7} Torr of pyridine pressure. The initial SH signal in Figure 2 was generated from the metal surface. Starting at about 120 K, the SH intensity increased dramatically and reached a saturation level at about 125 K. As previously reported from this laboratory,[18] this dramatic increase in the SH intensity after 120 K is indicative of crystallization in the pyridine film, i.e., the increase in the SH signal after 120 K originates from the crystalline phase in the pyridine film. The pyridine crystal belongs to the orthorhombic space group $Pna2_1$.[20] This space group is noncentrosymmetric, allowing SHG from the bulk of the crystallized film. Crystallization is a first-order phase transition and thus a well-defined transition temperature is expected. Observation of a broad transition temperature region

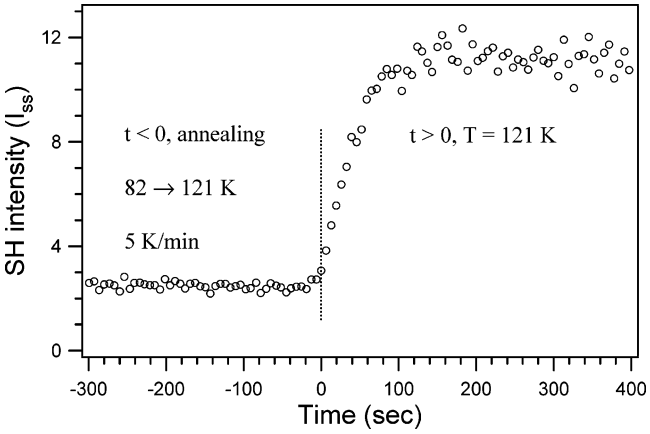

Figure 3. The SH intensity as a function of time during isothermal crystallization of a 70 nm thick pyridine film at 121 K. The pyridine film was originally grown at 82 K and then heated at 5 deg/min from 82 to 121 K ($t < 0$). From $t = 0$ the surface temperature was kept at 121 K.

in Figure 2 implies that crystallization in the film occurs through a diffusion-limited process (see Discussion).

Figure 3 shows the SH intensity as a function of time during isothermal crystallization at 121 K of a 70 nm thick amorphous pyridine film. The pyridine film was originally grown on Ag(111) at 82 K under 5×10^{-7} Torr of pyridine pressure and then heated at 5 deg/min from 82 to 121 K (the $t < 0$ region). From $t = 0$ the surface temperature was maintained at 121 K, the lowest temperature where discernible crystallization on the experimental time scale appeared. As described above, the amount of SH signal at $t < 0$ was from the metal surface only. The additional SH signal I_{ss} at $t > 0$ resulted from crystallization in the film and is proportional to the square of the fraction of crystalline phase in the film, f_{cryst}. According to the theory of isothermal crystallization kinetics, f_{cryst} scales exponentially with time as[21−23]

$$f_{cryst} = 1 - \exp(-kt^n) \quad (3)$$

where k is a time-independent constant in seconds^{-n}, and n is a parameter whose magnitude is determined by the geometry of the growing crystal domains in a diffusion-controlled process.

The square-root of the SH intensity with the initial value at 121 K subtracted, i.e., $(I_{ss})^{0.5}$, is plotted as a function of time in Figure 4. $(I_{ss})^{0.5}$ is proportional to f_{cryst} and is fitted to eq 3 with a proportionality factor, yielding $k = 0.08 \pm 0.01$ and $n = 0.8 \pm 0.05$.

C. SH Intensity from Annealed Pyridine Films as a Function of Temperature: Premelting of Crystallites. As the increase of the SH intensity from the film can be used to monitor the crystallization kinetics, its decrease can be used for examining the melting of the crystallites in the film. To explore this possibility, a 140 nm thick pyridine film was first grown on Ag(111) at 85 K and then annealed to 130 K to form a crystalline film. The SH intensity (open circles) from this crystalline film measured in the temperature range of 80 and 170 K is shown in Figure 5. The heating or cooling rates were set at 5 deg/min. It was found that between 80 and 140 K, the SH intensity increases with decreasing temperature. Significantly, the change in the SH intensity with temperature was found to be reversible in this temperature range. The reversibility holds true at all heating/cooling rates used in the experiments from 0.02 to 1 deg/s. Above 140 K, the SH intensity decays quickly and irreversibly with the increase of temperature.

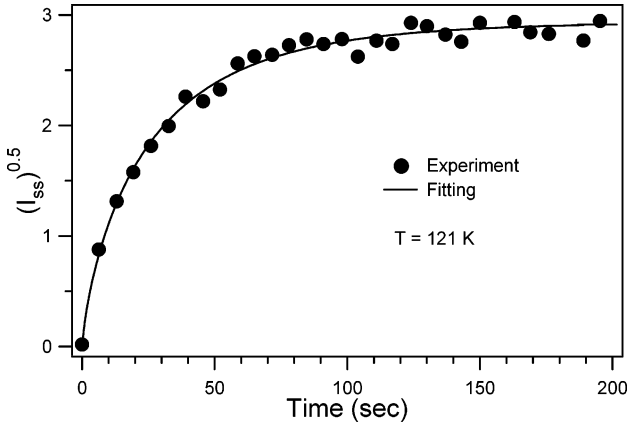

Figure 4. $(I_{ss})^{0.5}$ as a function of time. I_{ss} is obtained from the measured SH intensity in Figure 3 with the initial value at 121 K subtracted. Solid circles represent the experimental results and a solid line represents a fit to eq 3.

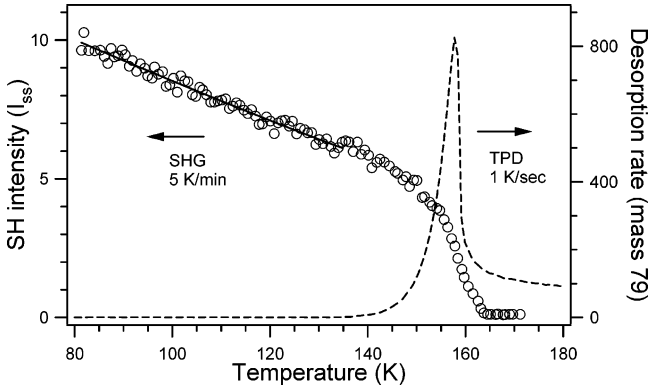

Figure 5. The SH intensity as a function of temperature detected from an annealed pyridine film on Ag(111). The heating/cooling rate was 5 deg/min. The 140 nm thick pyridine film was first annealed up to 130 K. Open circles are experimental results and the solid line is a fit to eq 5. The dashed line shows the temperature-programmed desorption curve of a 40 nm pyridine film (heating rate 1 K/s).

The decrease in the SH intensity from 80 to 140 K corresponds to a reduction of the fraction of crystalline phase in the film. The reversibility in the temperature dependence indicates a reversible phase transition—melting from crystalline solid to liquid and vice versa. The irreversible decrease above 140 K is the result of thermal desorption of the film. A TPD spectrum (shown as the dashed line in Figure 5) of a 40 nm thick pyridine film shows that the thermal desorption occurs starting at 140 K. The slow recovery of the baseline in the TPD spectrum above 165 K is due to slow pumping of the residual pyridine molecules in the UHV chamber.[24] The heating rate in the TPD study was 1 deg/s, faster than that (5 deg/min) used in the SHG measurement shown in Figure 4. In general, the peak position in the TPD spectrum shifts to lower temperature with slower heating rate.[25] Nonetheless, a calculation based on zero-order desorption kinetics found that thermal desorption below 140 K is negligible even at the heating rate of 0.02 deg/s.

IV. Discussion

Experimental observations indicate that the SHG technique can be used to monitor the growth and phase transitions of thin films made of pyridine molecules. The SHG results demonstrate that an amorphous pyridine film grown at 82 K undergoes crystallization at temperatures above 120 K. Time dependence of the SH intensity measured at a constant temperature of 121 K implies that crystallization is a diffusion-limited process leading to crystallites with cylindrical disk shapes. The SH intensity from a crystalline film was found to change reversibly with temperature in the range 80−140 K, indicating a melting−solidification phase transition over this broad temperature range. All these observations are consistent with previous conclusions,[18] deduced also from SHG studies, on the structure of annealed pyridine thin films. Here we discuss the correlation between the crystallization kinetics and the dimensionality of the crystallites, and the origin of the broad reversible phase transition for the crystalline film.

A. Crystallization Kinetics of Thin Pyridine Films. We have previously deduced from the azimuthal-angle dependence of SHG both from the pyridine films and from the bare Ag(111) that the annealed pyridine film is comprised of randomly oriented crystallites with an average size of more than 600 nm.[18] In their study, SHG from the clean metal surface showed a 6-fold symmetry pattern reflecting the C_{3v} symmetry of the (111) surface. The 6-fold symmetry pattern remained the same for the system of an amorphous pyridine film on Ag(111) as an amorphous pyridine film generates no SHG. On the other hand, they found that the azimuthal-angle dependence of SHG from the annealed pyridine films on Ag(111) contains an isotropic component that is absent from both the clean and amorphous pyridine film-deposited Ag(111). If the crystalline film were a single crystal, its symmetry (C_{2v} point group[20]) would facilitate an additional SHG component from the film that has a 4-fold symmetry pattern. This expectation is in contradiction with the observation of the isotropic component. On the basis of these observations, we have previously proposed that the annealed film is polycrystalline. Even though each crystallite has a directional susceptibility, they are randomly oriented with respect to the surface axes so that the overall sum of the susceptibility is isotropic in azimuthal-angle dependence. The fact that the sum of the individual crystallite susceptibility is nonzero infers that the average diameter of the polycrystallites is comparable to or larger than the coherence length for the SHG process, or $\geq$600 nm.[18]

Since the thickness of the films examined in their study was between 50 and 350 nm, it is intuitive to expect that the shape of the $\geq$600-nm diameter crystallites is a disklike cylinder, rather than being spherical. This deduction is consistent with the result obtained from the analysis of time-dependent SHG measurement reflecting the crystallization kinetics during isothermal crystallization of a 70 nm thick pyridine film. The analysis shows that the power parameter (n) in the crystallization rate is 0.8 ± 0.05. The exponent n is related to the geometrical dimension of the crystal domain in the crystallization process. In the diffusion-controlled process, $n = 1.5$, 1, and 0.5 for spherical, cylindrical, and plate-shaped crystal growth, respectively, while $n \geq 1$ in the case of the interface-controlled process.[22] The observed value, $n = 0.8 \pm 0.05$, therefore is consistent with a diffusion-controlled crystallization process and indicates that the shape of the crystal domains formed during the crystallization of the pyridine film at 121 K is somewhere between cylindrical and platelike.

Diffusion-limited crystallization in molecular films has been reported for ice on solid surfaces[21,26] and for styrene on a Pt surface.[23] Hage et al. reported diffusion-limited crystallization in a system of water film grown on the BaF_2 surface at 78 K in which amorphous water crystallizes to cubic ice in the temperature range of 140−150 K.[21] It was proposed that ice crystallizes in spherical geometry on BaF_2 flats but the film thickness was not specified in the report.[21] The system of pyridine film on

Ag is the only molecular film that we know of exhibiting a nonspherical crystallization mechanism. This perhaps is because in the systems we have examined the pyridine film thickness was kept thin enough that the weak intermolecular interaction would allow large domain crystallites to be formed. This observation shows clearly the influence of film thickness on the geometrical shape of the crystallite and the crystallization mechanism in molecular films.

B. Grain-Boundary Melting of Crystallites in Annealed Pyridine Films. The pyridine film grown at 82 K is amorphous and gives no SHG. The amorphous film anneals (crystallizes) at 123 K as indicated by the dramatic increase in the SH intensity generated. The annealing process is irreversible—when the temperature is lowered below 120 K the SH intensity does not decrease to the level of the metal surface. At this point, it is observed that the SH intensity from the annealed film changes reversibly with temperature (Figure 5). To ensure that the 40% decrease in the SH intensity from the film caused by a temperature change from 80 to 135 K is due to melting of the crystallites in the annealed film, we need to consider the effect of the following temperature-dependent physical properties: the film thickness, the SH intensity from the silver surface, and the size of the crystallites.

The thickness of the pyridine film may change with temperature due to thermal expansion/contraction. Although no experimental measurements on lattice constants as a function of temperature have been performed, molecular dynamics calculations[27] of pyridine crystal (orthorhombic) showed that the solid volume changes about 3% between 159 and 245 K. Experimental results for benzene (C_6H_6) and aniline (C_6H_7N) solids reported similar percentage changes in volume: A neutron diffraction study[28] of deuterated benzene solid (orthorhombic) reported that the solid volume changes 1.7% in thickness between 100 and 200 K. An X-ray diffraction study[29] of aniline solid (monoclinic) reported that lattice parameters changed less than 1% between 140 and 200 K. On the basis of these results, we estimate an ca. 2($\pm$1)% change in thickness of the polycrystalline pyridine film between 80 and 140 K and use this magnitude of change to estimate the effect on the SH intensity detected. As seen in Figure 1 and eq 1, the SH intensity from the metal surface propagating through the film is influenced by the film thickness due to interference. Assuming negligible change in refractive index, a 2% change in the film thickness would induce an estimated 4% change in SH intensity. This magnitude is much smaller than the observed value (40%) in Figure 5. Additional evidence indicating that the effect of thermal expansion on the SH intensity is negligible was found experimentally. If thermal expansion at increasing temperature induces significant changes in the SH intensity, it should increase (or decrease) at higher temperature for films thinner (or thicker) than 140 nm at which the SH intensity reaches the top of the first peak in Figure 1. We found, however, that the SH intensity always decreases with increasing temperature regardless of the film thickness.

It was observed that the SH intensity from the bare Ag(111) surface decreased by 10% when temperature was increased from 80 to 140 K. This magnitude of change, however, is negligible in comparison with the overall SH intensity change in Figure 5, particularly considering that the SH intensity from the metal surface is an order of magnitude smaller than that from the crystalline film, as seen in Figure 2. The reversible SH intensity change therefore is not associated with the metal surface.

Now we consider the influence of temperature on the size of the crystallites which will affect the SH intensity from the film. If the number density of the crystallites in the film is constant over the temperature range of interest, a reasonable assumption considering the average size of the crystallites is $\geq$600 nm, the SH intensity will decrease as the size of the crystallites becomes smaller. The size of the crystallites is affected by temperature both kinetically and thermodynamically. First from the viewpoint of kinetics, growth of the crystallites must be accelerated by increased temperature because crystallization of the pyridine film is diffusion-limited and diffusion rate increases with temperature. This would lead to an increase in the SH intensity with increasing temperature. This expectation, however, does not agree with the observation.

We propose that the reversible temperature dependence of the SH intensity in the range of 80−135 K in Figure 5 is the result of the *reversible* change in the size of the crystallites. The change in crystallite size results from thermodynamic equilibrium between the solid crystalline and disordered liquid phases in which the crystallite is subjected to grain-boundary melting. Grain-boundary, or interfacial, melting occurs when the formation of a liquid skin between the crystal domains reduces the free energy of the system. The condition of grain-boundary melting is when $\sigma_{ss} \geq 2\sigma_{ls}$,[30] where σ_{ss} is the surface energy of a solid−solid boundary and σ_{ls} is the surface energy of a liquid−solid boundary. As temperature, T, approaches the bulk melting point of the solid, T_m, the liquid skin thickness, d_b, is expected to diverge as either $d_b = \log(T_m - T)$ or $(T_m - T)^{\beta}$, depending on the interfacial potentials.[31]

A model of grain-boundary melting is proposed here for an analytical description of the SHG results in Figure 5. Assuming that the liquid skin thickness is much smaller than the average radius of the crystallites, we can neglect the effect of curvature of the crystallite circumference on grain-boundary melting. The expression for grain-boundary melting of van der Waals solids is depicted by the thickness of the liquid layer d_b as[31]

$$d_b \propto \left(\frac{T_m}{T_m - T}\right)^{1/3} \tag{4}$$

If the number density of crystallites in the film does not change with temperature, as we limit the discussion to the situation of grain-boundary melting only, the SH intensity from the film is proportional to the square of the average volume of crystallites, V. In the grain-boundary melting process, the volume V is a function of temperature, $V = V_{max}[1 - d_b(T)/R]^m$, where m is a geometric order ($m = 3$ for spherical-shape crystallite and 2 for cylindrical-shape crystallite) and R is the maximum radius of a crystallite, i.e., when $d_b = 0$. Using eq 4 for $d_b(T)$ as $d_b = C[T_m/(T_m - T)]^{1/3}$ with a proportionality constant C, the measured SH intensity, $I^{2\omega}$, can be expressed as

$$I^{2\omega} = I^{2\omega}_{max}\left[1 - \frac{C}{R}\left(\frac{T_m}{T_m - T}\right)^{1/3}\right]^{2m} + I^{2\omega}_{o} \tag{5}$$

where $I^{2\omega}_{max}$ is the SH intensity from the pyridine film when $d_b = 0$ and $I^{2\omega}_{o}$ is the SH intensity from the metal surface. The solid line in Figure 5 represents a nonlinear least-squares fit to eq 5 with fixed parameters $T_m = 232$ K (the melting temperature of pyridine[32]) and $m = 2$. The latter is not a sensitive parameter for the fitting in such a narrow temperature range and is set because in the previous section it has been determined that the crystallization kinetics is one that mimics more of a cylindrical shape crystallite. It was found that the ratio d_b/R increases by 10% as temperature increases from 80 to 135 K. This means

that if $R = 300$ nm, liquid skin thickness increases by 30 nm with increasing temperature from 80 to 135 K.

Note that our fitting was performed in the temperature range of 80−135 K, of which the lowest temperature is set by the experimental limit and the highest one limited by thermal desorption of the film. Even though this analysis neglects the effect of the curvature of the crystallite and simply considers cylindrical-shaped crytallites ($m = 2$), the goodness of the fit clearly demonstrates the reasonableness of the model and the capability of the SHG technique for probing premelting in the ultrathin molecular films.

Understanding the physical properties of grain boundaries is important for designing characteristics aimed at enhancing performance in organic semiconductors because they may limit the mobility of charge carriers.[8,9,15] Our results suggest that since grain-boundary melting is a strong function of temperature, temperature dependence in electric/optical properties of ultrathin molecular films is expected.

Grain-boundary melting in molecular polycrystallites has been studied with use of NMR[33,34] and differential scanning calorimetry.[35,36] These techniques are informative for bulk samples but their effectiveness for studying thin molecular films, particularly the ones prepared in UHV environments, remains to be demonstrated. The SHG technique on the other hand is shown to be capable of real-time monitoring of the premelting process of polycrystallites, providing more precise analysis for understanding thin molecular films.

V. Conclusion

Pyridine is a small molecule with a rather typical disklike shape so that it can be used as a model system for understanding the structure and properties of thin molecular films made of molecules with very weak intermolecular interactions. Previously a study using thermal desorption spectroscopy[24] has shown that the deposition of the film from the first layer on substrate to the film bulk goes through a metastable layer that results from faster diffusion of molecules between layers, consistent with the very weak intermolecular interaction. A previous second harmonic generation study[18] has shown that the bulk film deposited at low temperature (below 120 K) is amorphous, but anneals at temperatures higher than 120 K to form crystallized domains with sizes $\geq$600 nm.

In this study it has been shown that second harmonic generation can be used to characterize the properties of the crystallites in the molecular films with thickness ~100 nm. It is found that the crystallites are formed in the annealing process at $\geq$120 K through a diffusion-limited crystallization process, with the crystalline domain growing with a shape somewhere between a plate and a cylinder. This finding, deduced from the observed second harmonic intensity generated from the film during the crystallization process, is consistent with the diameter and thickness of crystallite domains determined previously and suggests that film thickness is an important factor in determining the crystallization mechanism. The present study also finds that the boundary of the crystalline domain crystallizes or melts as the temperature is decreased or increased even in the range of 80−135 K, much lower than the bulk melting temperature (232 K).

These observations and analysis seem to point to a model for the growth of thin films made of molecules with very weak intermolecular interactions: The very weak intermolecular potential does not provide sufficient energy for the molecules deposited onto the film to rotate and translate into positions to form crystallized structure. As the temperature is raised, in the case of pyridine it is around 120 K when the molecules gain sufficient energy to crystallize. Under the conditions that the film thickness is about 100 nm, the crystallites are formed through a shape between plate and cylinder and eventually in a cylindrical disk shape with micron diameters. The axes of these crystallites are randomly oriented on the surface. After annealing, molecules at the crystallite boundary would further crystallize at decreased temperature and melt at increased temperature until the desorption temperature of the bulk film is reached.

Acknowledgment. This work is supported by a grant from the Air Force Office of Scientific Research. The use of equipment supported by the National Science Foundation MRSEC Program, no. DMR00-79909, is acknowledged.

References and Notes

(1) Schoonveld, W. A.; Wildeman, J.; Fichou, D.; Bobbert, P. A.; van Wees, B. J.; Klapwijk, T. M. *Nature* **2000**, *404*, 977.
(2) Dodabalapur, A.; Torsi, L.; Katz, H. E. *Science* **1995**, *268*, 270.
(3) Peumans, P.; Bulovic, V.; Forrest, S. R. *Appl. Phys. Lett.* **2000**, *76*, 3855.
(4) Granstrom, M.; Petritsch, K.; Arias, A. C.; Lux, A.; Andersson, M. R.; Friend, R. H. *Nature* **1998**, *395*, 257.
(5) Sheats, J. R.; Antoniadis, H.; Hueschen, M.; Leonard, W.; Miller, J.; Moon, R.; Roitman, D.; Stocking, A. *Science* **1996**, *273*, 884.
(6) *Nonlinear Properties of Organic Molecules and Crystals*; Chemla, D. S., Zyss, J., Eds.; Academic: New York, 1989; Vols. 1 and 2.
(7) Forrest, S. R. *Chem. Rev.* **1997**, *97*, 1793.
(8) Heringdorf, F. M.; Reuter, M. C.; Tromp, R. M. *Nature* **2001**, *412*, 517.
(9) Dimitrakopoulos, C. D.; Kymissis, I.; Purushothaman, S.; Neumayer, D. A.; Duncombe, P. R.; Laibowitz, R. B. *Adv. Mater.* **1999**, *11*, 1372.
(10) Adamson, A. W.; Gast, A. P. *Physical chemistry of surfaces*, 6th ed.; Wiley-Interscience: New York, 1997.
(11) *Handbook of micro/nano tribology*, 2nd ed.; Bhushan, B., Ed.; CRC Press: Boca Raton, FL, 1999; Vol. 1.
(12) Bhushan, B.; Israelachvili, J. N.; Landman, U. *Nature* **1995**, *374*, 607.
(13) Marx, D.; Wiechert, H. *Adv. Chem. Phys.* **1996**, *95*, 213.
(14) Horowitz, G.; Hajlaoui, R.; Fichou, D.; Kassmi, A. E. *J. Appl. Phys.* **1999**, *85*, 3202.
(15) Northrup, J. E.; Tiago, M. L.; Louie, S. G. *Phys. Rev. B* **2002**, *66*, 121404.
(16) Sagarik, K.; Spohr, E. *Chem. Phys.* **1995**, *199*, 73.
(17) Li, C. M.; Ying, Z. C.; Dai, H. L. *J. Chem. Phys.* **1994**, *101*, 7058.
(18) Sjodin, T.; Troxler, T.; Dai, H. L. *Langmuir* **2000**, *16*, 2832.
(19) Avouris, P.; Demuth, J. E. *J. Chem. Phys.* **1981**, *75*, 4783.
(20) Mootz, D.; Wussow, H. G. *J. Chem. Phys.* **1981**, *75*, 1517.
(21) Hage, W.; Hallbrucker, A.; Mayer, E.; Johari, G. P. *J. Chem. Phys.* **1994**, *100*, 2743.
(22) Doremus, R. H. *Rates of Phase Transformations*; Academic Press: New York, 1985.
(23) Bai, J.; Snively, C. M.; Delgass, W. N.; Lauterbach, J. *Macromolecules* **2001**, *34*, 1214.
(24) Yang, M. C.; Rockey, T.; Pursell, D.; Dai, H. L. *J. Phys. Chem. B* **2001**, *105*, 11945.
(25) Redhead, P. A. *Vacuum* **1962**, *12*, 203.
(26) Smith, R. S.; Huang, C.; Wong, E. K. L.; Kay, B. D. *Phys. Rev. Lett.* **1997**, *79*, 909.
(27) Gamba, Z.; Klein, M. L. *Chem. Phys.* **1989**, *130*, 15.
(28) Craven, C. J.; Hatton, P. D.; Howard, C. J.; Pawley, G. S. *J. Chem. Phys.* **1993**, *98*, 8236.
(29) Fukuyo, M.; Hirotsu, K.; Higuchi, T. *Acta Crystallogr. B* **1982**, *38*, 640.
(30) Schick, M.; Shih, W. *Phys. Rev. B* **1987**, *35*, 5030.
(31) Dash, J. G.; Fu, H.; Wettlaufer, J. S. *Rep. Prog. Phys.* **1995**, *58*, 115.
(32) *CRC Handbook of Chemistry and Physics*, 83rd ed.; Lide, D. R., Ed.; CRC Press: Boca Raton, FL, 2003.
(33) Dosseh, G.; Fressigne, C.; Fuchs, A. H. *J. Phys. Chem. Solids* **1992**, *53*, 203.
(34) Rousseau, B.; Bessada, C.; Fuchs, A. H. *Solid State Commun.* **1988**, *67*, 1017.
(35) Demirjian, B. G.; Dosseh, G.; Chauty, A.; Ferrer, M.; Morineau, D.; Lawrence, C.; Takeda, K.; Kivelson, D. *J. Phys. Chem. B* **2001**, *105*, 2107.
(36) Wilson, P. W.; Arthur, J. W.; Haymet, A. D. J. *Biophys. J.* **1999**, *77*, 2850.